Lithium 1s main-line and satellite photoemission: Resonant and nonresonant behavior

T. A. Ferrett,* D. W. Lindle,* P. A. Heimann,† W. D. Brewer,‡ U. Becker,§
H. G. Kerkhoff,§ and D. A. Shirley
Materials and Chemical Sciences Division, Lawrence Berkeley Laboratory and Department of Chemistry, University of California, Berkeley, California 94720
(Received 13 March 1987)

We present experimental results on core-level photoemission of atomic lithium, leading to both main-line and satellite states of the Li^+ ion ($1snl$ where $n=2-5$). We compare the measured $1s2s\ ^{1,3}S$ main-line cross sections with recent relaxed Hartree-Fock calculations and with previous experimental results, finding reasonable agreement in both cases. For the $n=3$ satellite, our results disagree with earlier photoemission work which was complicated by additional peaks at 52 eV kinetic energy. We discuss possible explanations for these extra peaks. For the doubly excited state $1s(3s3p)$ at 71.14 eV, we present total cross-section results in good agreement with previous photoabsorption measurements. The qualitative differences among our partial cross-section profiles are discussed, and the phase for the total cross section is rationalized by estimating the signs of pertinent matrix elements.

I. INTRODUCTION

The study of electron-correlation effects on the photoionization of small atoms is important for two reasons. First, the accessibility of small atoms to the most sophisticated *ab initio* theoretical treatments, coupled with the high sensitivity of photoionization processes to multielectron effects, can lead to a better understanding of basic electron-correlation phenomena. Second, experience with small atoms can provide insight into photoionization processes in larger atoms and molecules. In helium, the smallest atom in which electron correlation can occur, both resonant and nonresonant experimental studies,[1–12] coupled with theory,[13–22] have elucidated the role of electron correlation in the continuum with respect to the $He^+(2s)$ and $He^+(2p)$ satellite channels.

In this paper we report photoelectron spectroscopic studies on the next smallest system, atomic lithium. We emphasize in this work the Li 1s satellite states, for which open shells and electron correlation in both initial and final states can further complicate photoionization processes relative to atomic helium.

Though the valence ionization of atomic Li has been studied extensively,[23–25] relatively little experimental work has been reported on core photoionization for the $Li^+(1s2s\ ^{1,3}S)$ main lines and $1snl$ satellites. Figure 1 depicts these pertinent energy levels in Li and Li^+, including the $1s(3s3p)$ doubly excited state of the neutral. Photoabsorption measurements have provided information on some of the $n=2$ satellites,[26] and on the energies and assignments of the resonances leading to the main-line and higher-satellite thresholds.[27–30] A recent work on core-level photoemission results for Li was complicated by unexplained peaks which were tentatively ascribed to the presence of a significant amount of molecular Li_2 in the effusive gas beam.[31]

Several theoretical papers have addressed the 1s ionization in Li, either at one or two photon energies[32] or at the sudden limit.[33] Recent relaxed Hartree-Fock results have been reported on the photoemission cross sections as a function of energy for the 1s main lines $1s2s\ ^{1,3}S$.[34] Comparison of experimental results with this theory should indicate the reliability of calculations at this level, and possibly test the importance of electron-correlation effects in the simplest open-shell atom. Unfortunately, the available photoemission spectra[31,35] contain unexplained peaks at ~ 52 eV kinetic energy as noted above. These peaks are assigned to Auger electrons emitted from decay of the core-ionized dimer, as mentioned above,[35] but Larkins *et al.*[36] have questioned this interpretation.

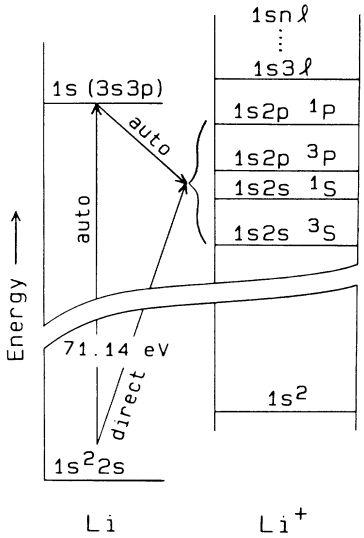

FIG. 1. Energy-level diagram for neutral and singly ionized lithium. Binding energies are listed in Table I. At the doubly excited state $1s(3s3p)$ at 71.2 eV, the autoionizing decay channels to the $n=2$ manifold ($1s2l$) are shown.

We report here on core-level photoemission spectra for the atomic Li main lines and $1snl$ satellites where $n=2-5$. Our experimental spectra are unambiguous because they contain no unexplained peaks. For our nonresonant results, we compare to the relaxed Hartree-Fock calculations of Larkins *et al.*,[34] and to previous experimental results.[31,35] For the "Auger" peaks in the data of Krummacher *et al.*[31] and Gerard,[35] we also discuss an alternate explanation due to Larkins *et al.*[36] which involves atom- and/or ion-molecule collisions followed by autoionization. If this interpretation is correct, the photoemission cross sections given by Gerard[35] should be reanalyzed with no adjustment for molecular Li_2.

Additional information on electron-correlation satellites in simple systems can be obtained from resonant excitation to these states. Along these lines and in analogy to the $3s3p$ excited state in neutral He, we report on the doubly excited resonance in $Li[1s(3s3p)^3P]^2P$ at 71.14 eV.[37] At this resonance, we have measured cross-section profiles for the $1s$ main lines and $n=2$ satellites ($1s2p\ ^{1,3}P$). Total cross-section measurements[26,30] indicating some asymmetry to the shape of the resonant profile were confirmed by our results which ascribe this asymmetry to the individual main-line ($1s2s\ ^{1,3}S$) profiles only.

Section II describes our experiment. Nonresonant and resonant results are given in Secs. III and IV, respectively. Conclusions appear in Sec. V.

II. EXPERIMENTAL PROCEDURE

The atomic Li photoemission experiment was performed at the Stanford Synchrotron Radiation Laboratory (SSRL) on Beamline III-1, using a grazing-incidence "grasshopper" monochromator. Relative cross sections and branching ratios were measured with a time-of-flight (TOF) electron analyzer at the "magic angle" of $\theta=54.7°$ relative to the photon polarization direction, as described previously.[38–40] A second TOF detector was placed at $\theta=0°$ with the goal of determining the angular distribution asymmetry parameters (β). Because of low counting rates together with oven instability due to the buildup of Li and other factors, the β values for the main lines and satellites could not be reliably determined by calibration with rare gases.

The TOF detectors were modified by insertion of a retarding grid at the beginning of the flight path. The experiment was performed with a 2-V retarding potential on this grid, to cut off thermally produced low-energy electrons from the oven. The 54.7° analyzer transmission was calibrated as a function of kinetic energy using the known partial cross sections for Ne $2s$ and $2p$ photoemission.[41]

A resistively heated metal vapor oven constructed of molybdenum was used to produce an effusive beam of Li, as described previously,[42–43] with several modifications. The running temperature was ~575 °C, where the Li backing pressure in the sample cup behind the nozzle was ~0.03 torr.[44] About 140 W were needed to reach this temperature, with the power divided among three resistive heating wires, two on the oven body and one on the nozzle. To help prevent bumping, small tantalum chips were inserted into the sample cup with solid Li. A slightly modified skimmer and skimmer standoff were used to prevent buildup of condensed Li before the skimmer exit.

At 575 °C, only ~1% of the metal-vapor beam is molecular Li_2, according to thermodynamic calculations by Nesmeyanov.[44] We saw no evidence of Li_2 Auger lines in the 40–55-eV kinetic energy range, in contrast to the peaks observed by Krummacher *et al.*[31] and Gerard[35] at ~52 eV kinetic energy.

During the collection of the nonresonant spectra, the oven pressure was unstable. Thus, branching ratios were measured, showing excellent agreement between two separate experimental runs. Averaged results are presented in Sec. III A. The monochromator bandpass was 0.30–0.50 eV for the nonresonant work.

For the resonant spectra, the oven was stable enough to measure relative partial cross sections. The monochromator resolution was 0.20(3) eV full width at half maximum (FWHM). The spectral intensities were normalized to the incident photon beam using electron yield measurements from a stainless-steel grid mounted in the beam line. Small pressure variations (less than 10%) as a function of time were accounted for by returning to a reference photon energy (71.2 eV) every third spectrum.

A 1000-Å-thick silicon window isolated the monochromator (10^{-9} torr) from the sample chamber (10^{-6} torr). The monochromator energy calibration was obtained from the energy positions of the atomic resonances in Li ($1s3s3p$ at 71.14 eV),[37] He ($3s3p$ at 69.92 eV),[8] and Xe ($4d_{5/2}\rightarrow 6p$ at 65.11 eV).[45]

A representative TOF photoelectron spectrum is shown in Fig. 2, taken at $\theta=54.7°$ and $h\nu=87$ eV, above the satellite thresholds. The main-line and satellite binding energies are reported in Table I.

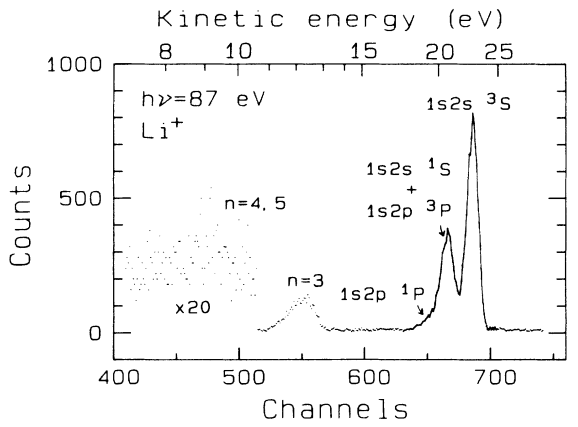

FIG. 2. TOF photoelectron spectrum taken at $h\nu=87$ eV and $\theta=54.7°$. The $1s2s$ main-line photoemission is split into ^3S and ^1S components, with the $1s2p\ ^{1,3}P$ satellites unresolved at slightly higher binding energy. The relatively intense $n=3$ satellites ($1s3l$) have a binding energy of about 75 eV (Ref. 64). The very weak higher n satellites are shown also on an expanded scale ($\times 20$).

TABLE I. Binding energies for the main-line and satellite photoemission lines in atomic lithium.

Li^+ configuration	Binding energy (eV)[a]
Main lines	
$1s^2$	5.390
$1s2s\ ^3S$	64.41
$1s2s\ ^1S$	66.15
$n=2$ satellites	
$1s2p\ ^3P$	66.67
$1s2p\ ^1P$	67.61
$n=3$ satellites	
$1s3s\ ^3S$	74.17
$1s3s\ ^1S$	74.67
$1s3p\ ^3P$	74.76
$1s3p\ ^1P$	75.04
$n=4$ satellites[b]	
$1s4s\ ^3S$	77.30
$n=5$ satellites[b]	
$1s5s\ ^3S$	78.69

[a]From Ref. 64.
[b]For simplicity, we list only the $ns\ ^3S$ channel.

III. NONRESONANT RESULTS

The nonresonant branching ratios for Li ionization to the $1s2l$ and $1s3l$ final states are presented in Sec. III A and compared with other experimental measurements and theory. The absolute cross sections are derived in Sec. III B, where the results are also compared with experiment and theory.

A. Branching ratios

We have measured branching ratios related to the $n=2$ ($1s2l$) ionization of Li as follows: $\sigma(^1P)/\sigma(^3S)$ (72–80 eV), $\sigma(^3S)/\sigma(^1S+^1P+^3P)$ (75–92.5 eV), and $\sigma(^3S)/\sigma(^1S+^3P)$ (75–77.5 eV). These are included in Table II, along with the derived ratio $\sigma(^3S)/\sigma(^1S+^3P)$ for $h\nu \geq 80$ eV.

In Fig. 3 we show the $\sigma(^1P)/\sigma(^3S)$ ratio from our work and that of Gerard.[35] Above 80 eV, the ^1P satellite was unresolved from the main lines in our spectra. Agreement between the two experimental data sets is good, despite some uncertainties associated with the data of Gerard caused by possible molecular Li_2 contributions to their spectra.[31,35] No published theoretical predictions for either of the $n=2$ shakeup satellites at these energies are available for comparison. However, preliminary Hartree-Fock results by Richards[17] found the ratio $\sigma(^1P)/\sigma(^3S)$ to be 0.07–0.15, depending on the form of the dipole operator. The data lie mostly in this range.

The $\sigma(^3S)/\sigma(^1S+^{1,3}P)$ ratio shown in Fig. 4 (top) is relatively constant over the measured range. Of more interest is the $\sigma(^3S)/\sigma(^1S)$ branching ratio, for which theoretical calculations are available.[34] Because we did not resolve the ^3P satellite from the ^1S main line in our TOF spectra, we show in Fig. 4 (bottom) the ratio

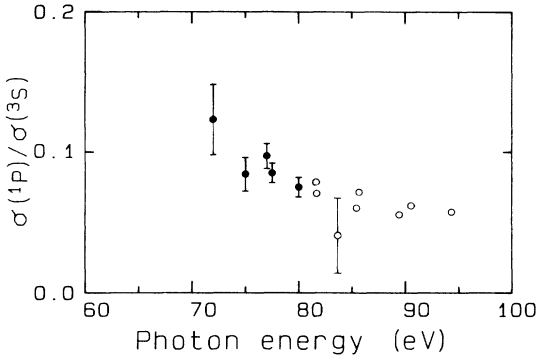

FIG. 3. Experimental $n=2$ ($1s2l$) branching ratio $\sigma(^1P)/\sigma(^3S)$. Experimental results by Gerard (Ref. 35) (with a representative error bar) are shown by open circles, and our data by dark circles.

$\sigma(^3S)/\sigma(^1S+^3P)$. From the range $h\nu=75$–77.5 eV, we have measured this ratio directly. At 80 eV and higher in energy, we have derived it from the measured $\sigma(^3S)/\sigma(^1S+^{1,3}P)$ and $\sigma(^1P)/\sigma(^3S)$ ratios as follows. At all energies,

$$R_c=\sigma(^3S)/\sigma(^1S+^3P)=(1/R_{31}-R_p)^{-1}\ , \qquad (1)$$

where $R_{31}=\sigma(^3S)/\sigma(^1S+^{1,3}P)$ and $R_p=\sigma(^1P/^3S)$. In the range 80 eV $\leq h\nu \leq$ 92.5 eV, we have used the mea-

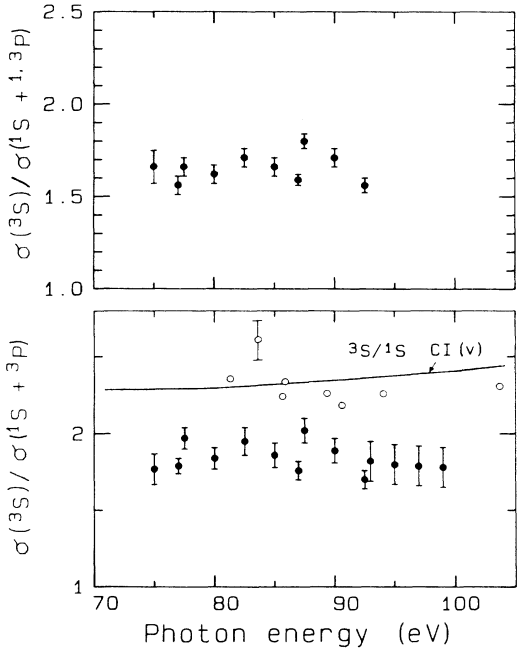

FIG. 4. Experimental $n=2$ ($1s2l$) branching ratio $\sigma(^3S)/\sigma(^1S+^{1,3}P)$ (top) and derived branching ratio $\sigma(^3S)/\sigma(^1S+^3P)$ (bottom). Solid circles are our results. Open circles are those of Gerard (Ref. 35) for $\sigma(^3S)/\sigma(^1S)$. Theory curve in the bottom panel is the Hartree-Fock velocity (V) result (Ref. 34) for the $\sigma(^3S)/\sigma(^1S)$ ratio.

sured values for R_{31} and assumed a linear decrease for the $R_p(^1P/^3S)$ ratio as stated in Table II and consistent with the results of Gerard.[35] For $h\nu \geq 93$ eV, we have used a value for the R_{31} ratio which is an average of those measured for $h\nu = 75$–92.5 eV. This, combined with the assumption mentioned above for R_p, results in the values in brackets in Table II for R_c and in Fig. 4 (bottom).

Also included in Fig. 4 (bottom) are the theoretical values for $\sigma(^3S)/\sigma(^1S)$.[34] The theory predicts this ratio to be nonstatistical and nearly constant over the range of our experiment. Our data include the ^3P satellite in the denominator of the ratio, and should therefore lie below the theoretical curve.

The Gerard data[35] for the $\sigma(^3S)/\sigma(^1S)$ ratio, also shown in Fig. 4, are systematically higher than ours, as expected. With the use of the theoretical value for $\sigma(^3S)/\sigma(^1S)$, we find that the ratio $\sigma(^3P)\sigma/(^3S)$ is about 0.14(4), in accordance with the results of Gerard.[35] This result also implies that perhaps 26(8) percent of the $(^1S + ^3P)$ peak intensity in our spectra is associated with the $1s2p\ ^3P$ satellite. We note that preliminary Hartree-Fock (HF) calculations[18] indicate a $\sigma(^3P)/\sigma(^3S)$ ratio of 0.24 at $h\nu = 90$ eV from the "length" approximation. However, the "velocity" results[18] predict negligible intensity for the ^3P satellite. Higher-resolution work is needed to establish the intensity of this conjugate shake-up satellite as a function of energy.

For ionization to the $1s3l$ states, we plot the $\sigma(n=3)/\sigma(n=2)$ $[\sigma(1s3l)/\sigma(1s2l)]$ branching ratio in Fig. 5, and set out the numerical results in Table III. The ratio increases slightly with energy. One point from Krummacher *et al.*[31] is shown also in Fig. 5. These authors noted possible problems with the correction for molecular Li_2. We defer comparison with the Gerard data[35] to the next section on absolute cross sections. Again, there are no published calculations for the energy dependence of the $n=3$ satellite intensity. Preliminary HF theory yields the $\sigma(n=3)/\sigma(n=2)$ ratio at 90 eV as 0.33 for the velocity results and 0.50 for the length results.[18] Early theoretical work at $h\nu = 151$ eV calculated the $\sigma(n=3)/\sigma(n=2)$ ratio to be 0.22–0.25, depending on the degree of configuration interaction included.[32] Sudden-limit calculations for the $\sigma(1s3s\ ^1S)/\sigma(1s2s\ ^1S)$ ratio give a value of 0.33.[33]

Several high-intensity spectra were taken, permitting measurement of the $1snl$ $(n=4,5)$ intensity relative to the $n=3$ satellites. Most of the integrated intensity for the higher satellites is probably due to $n=4,5$ states because the cross section for the higher satellites drops dramatically with n.[46,47] This ratio $\sigma(n=4,5)/\sigma(n=3)$ between 87 and 93 eV was 0.07(2), which corresponds to a $\sigma(n=4,5)$ intensity of about 1.7(4)% relative to the $n=2$ ionization manifold. The only theoretical results available for comparison are HF calculations by Larkins *et al.*[32] which predict the $\sigma(n=4,5)/\sigma(n=3)$ ratio to be 1–4% at $h\nu = 151$ eV, somewhat below experiment. Sudden-limit results[33] for the ratio $\sigma(1sns;\ n=4,5)/\sigma(1s2s\ ^{1,3}S)$ give a value of about 1.3%, in good agreement with our results.

B. Absolute cross sections

From our branching ratios in Tables II and III and the total photoabsorption cross section, σ(total), taken from Fig. 1 of Ref. 30, we have derived the absolute cross sections $\sigma(n=2)$, $\sigma(n=3)$, $\sigma(1s2s\ ^3S)$, and $\sigma(1s2s\ ^1S + 1s2p\ ^3P)$ set out in Table IV. We note that the quoted absolute accuracy of the photoabsorption data[30] is 20%, and is not included in the errors shown in

TABLE II. Experimental branching ratios for lithium $n=2$ photoionization.

Photon energy (eV)	R_{31} $\sigma(^3S)/\sigma(^1S + ^{1,3}P)$	R_c $\sigma(^3S)/\sigma(^1S + ^3P)$[a]	R_p $\sigma(^1P)/\sigma(^3S)$
72[b]			0.123(25)
75	1.66(9)	1.77(10)	0.084(12)
77	1.56(5)	1.79(5)	0.097(9)
77.5	1.66(5)	1.97(7)	0.085(7)
80	1.62(5)	1.84(7)	0.075(7)
82.5	1.71(5)	1.95(9)	
85	1.66(5)	1.86(8)	
87	1.59(3)	1.76(6)	
87.5	1.80(4)	2.02(8)	
90	1.71(5)	1.89(8)	
92.5	1.56(4)	1.70(6)	
93		[1.82(13)][c]	
95		[1.80(13)]	
97		[1.79(13)]	
99		[1.78(13)]	

[a]For $h\nu < 80$ eV, this ratio was measured directly. For $h\nu \geq 80$ eV, this ratio was derived by assuming that the ratio $R_p(\sigma(^1P)/\sigma(^3S))$ behaves linearly above 80 eV according to the equation $R_p = -0.18[h\nu(\text{eV})] + 21.9$ with an uncertainty of ± 0.15.

[b]In the vicinity of the resonances leading to the $n=3$ satellite thresholds.

[c]The numbers in brackets [ ] were derived using a value for $\sigma(^3S)/\sigma(^1S + ^{1,3}P)$ which is an average of the values in column 1 [1.65(10)].

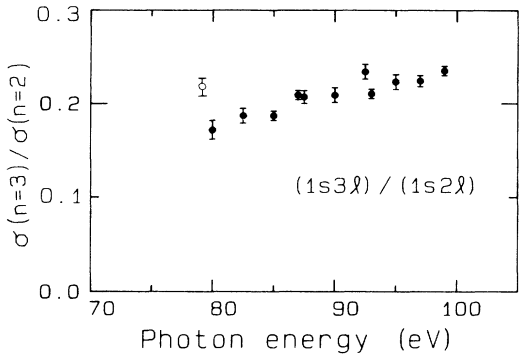

FIG. 5. Experimental branching ratio $\sigma(n=3)/\sigma(n=2)$ ($1s3l/1s2l$). One experimental point by Krummacher *et al.* (Ref. 31) is shown (open circle).

our plots.

We now discuss how the absolute cross-section values were obtained. At each photon energy, the following relations hold:

$$\sigma(n=2)=\sigma(\text{total})/(1+R)\ , \tag{2}$$

$$\sigma(n=3)=\sigma(\text{total})-\sigma(n=2)\ , \tag{3}$$

where $R=\sigma(n=3)/\sigma(n=2)$ and assuming that the only significant contributions to the total cross section come from the $n=2$ and $n=3$ ionization manifolds. We have neglected ionization of the $2s$ electron, which contributes only 1–2 % to the σ(total) at these energies,[34,35] and the intensity of the higher n satellites ($n\geq 4$). Thus, $\sigma(n=2)$ and $\sigma(n=3)$ were calculated from Eqs. (2) and (3), respectively, for $h\nu\geq 80$ eV. At two additional lower photon energies (75 and 77.5 eV), $\sigma(n=2)$ was obtained directly from the relative cross-section measurements taken while the metal-vapor oven was stable for a short period, and scaled at 80 eV to the absolute values derived above.

The values for $\sigma(1s2s\ ^3S)$ can be expressed in terms of measured and derived branching ratios as

$$\sigma(1s2s\ ^3S)=\sigma(n=2)R_c/[1+R_c(1+R_p)]\ , \tag{4}$$

where R_c is defined in Eq. (1) and found in column 3 of Table II, and R_p is either as measured or assumed as stated in Table II. Finally, $\sigma(^1S+^3P)$ was calculated as

$$\sigma(^1S+^3P)=\sigma(^3S)/R_c\ . \tag{5}$$

Uncertainties in all cross sections in Table IV were derived from the statistical uncertainties in the measured branching ratios and in the assumption for R_p (see Table II).

We now compare the derived absolute cross sections with the experimental results of Gerard[35] and theoretical results where available. In Fig. 6 our $\sigma(n=2)$ is plotted along with the data of Gerard,[35] showing the expected decrease from threshold for ionization of a $1s$ electron. The overall agreement between the two data sets is fairly good, though the slope of the decrease with energy is somewhat different. No theoretical curves have been plotted because there are as yet no published calculations on the energy-dependent behavior of the $1s2p$ conjugate satellites.

The reliability of present theory can be assessed by

TABLE III. Experimental branching ratio $\sigma(n=3)/\sigma(n=2)$ [$\sigma(1s3l)/\sigma(1s2l)$] for lithium photoionization.

Photon energy (eV)	$\sigma(n=3)/\sigma(n=2)$
80	0.172(10)
82.5	0.187(8)
85	0.187(5)
87	0.209(5)
87.5	0.207(7)
90	0.209(8)
92.5	0.234(8)
93	0.210(5)
95	0.223(8)
97	0.224(6)
99	0.235(5)

TABLE IV. Absolute cross sections (Mb) derived for lithium $n=2$ ($1s2l$) and $n=3$ ($1s3l$) photoionization. See text for details of derivation. The errors shown parenthetically are statistical. In addition, the total cross-section data from Ref. 30, on which the absolute scale is based, have an absolute error of 20%.

Photon energy (eV)	$\sigma(n=2)$	$\sigma(n=3)$	$n=2$ $\sigma(^3S)$	$n=2$ $\sigma(^1S+^3P)$
75	1.99(8)		1.21(11)	0.69(7)
77.5	1.90(8)		1.19(10)	0.60(5)
80	1.86(2)	0.32(2)	1.15(7)	0.63(5)
82.5	1.67(2)	0.31(2)	1.05(7)	0.54(4)
85	1.58(1)	0.30(1)	0.99(7)	0.53(4)
87	1.45(1)	0.30(1)	0.89(5)	0.51(3)
87.5	1.43(1)	0.29(1)	0.92(6)	0.46(4)
90	1.41(1)	0.29(1)	0.89(6)	0.47(4)
92.5	1.30(1)	0.31(1)	0.79(4)	0.46(3)
93	1.29(1)	0.27(1)	0.81(9)	0.45(6)
95	1.28(1)	0.28(1)	0.80(9)	0.44(6)
97	1.18(1)	0.27(1)	0.74(8)	0.41(5)
99	1.09(1)	0.26(1)	0.68(8)	0.38(5)

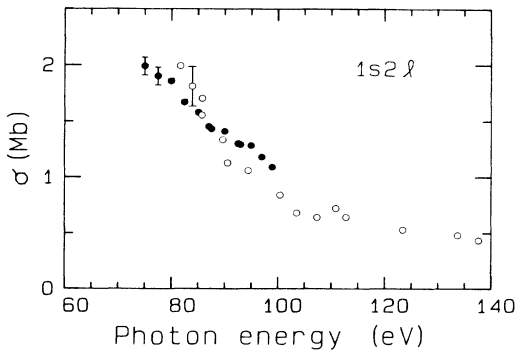

FIG. 6. Derived absolute cross section (Mb) for $n=2$ ($1s2l$) photoionization. Open circles are experimental results by Gerard (Ref. 35) with a representative error bar.

comparing the individual cross sections for the $n=2$ ($1s2l$) main lines. In Fig. 7 the $1s2s\ ^3S$ partial cross section is shown with the data of Gerard[35] and theoretical curves from Larkins *et al.*[34] We note that the preliminary theoretical results by Richards[18] are also in agreement with those plotted in Fig. 7. Only the velocity results of the theory are plotted, though the velocity and length forms agree within $\sim 10\%$. Both relaxed Hartree-Fock (RHF) and configuration-interaction (CI) results are shown, with the CI calculation producing consistently lower values by $\sim 8\%$ relative to the RHF results. Both curves predict an energy dependence of the cross section in good agreement with our results. Again, Gerard's data drop off more quickly above $h\nu = 80$ eV than either theory or our data.

For the $1s2s\ ^1S$ main line, Fig. 8 shows Gerard's data[35] and both RHF and CI velocity forms of theory, along with our summed results for the unresolved ^1S main line and ^3P satellite. Early calculations by Richards[18] agree with the plotted theory. Whereas our ^3S main-line cross section was slightly lower than theory (Fig. 7), our $^1S + {}^3P$ values are slightly higher, presumably due to the ^3P contribution. As discussed previously, about 26(8)% of this summed intensity is due to the satellite if the theory predicts the $^3S/{}^1S$ ratio correctly. The energy dependence in our data is well modeled by theory.

Finally, for the $n=3$ ($1s3l$) satellites, Fig. 9 shows the derived absolute cross sections from our experiment and Gerard's.[35] Here we find the largest discrepancy between the two experimental data sets. The agreement is poor and becomes increasingly worse especially to lower energy, where the data of Gerard rises steeply. At ~ 82 eV, the difference between the two sets is about a factor of 2. The only nonstatistical uncertainty in the overall shape of our results stems from decreasing detector transmission when the $n=3$ satellite is at low kinetic energy. We believe that we have adequately accounted for this effect because $\sigma(n=3)$ derived from two separate experimental runs, with different transmission corrections, were in excellent agreement.

In trying to understand this disagreement for $\sigma(n=3)$, and similar variance noted earlier, we must consider complications in Gerard's experiment, which may have implications for all of Gerard's data presented in Figs. 3–9 and discussed above. Additional peaks at 51.6 and 52.8 eV kinetic energy were observed in the photoelectron spectra.[31,35] These peaks were totally absent in our spectra. They have been interpreted as the Li_2 Auger transitions shown below because they do not shift in kinetic energy as the photon energy is scanned:[35]

$$Li_2^+(1\sigma_u^{-1}1\sigma_g^2 2\sigma_g^2) \rightarrow Li_2^{2+}(1\sigma_u^2 1\sigma_g^2) + e^-_{\text{Auger}}\ , \quad (6)$$

$$Li_2^+(1\sigma_u^2 1\sigma_g^{-1} 2\sigma_g^2) \rightarrow Li_2^{2+}(1\sigma_u^2 1\sigma_g^2) + e^-_{\text{Auger}}\ . \quad (7)$$

Corrections were made to the data by subtracting the inferred concommitant Li_2 photoelectron intensity arising from the $1s$ ionization.[31,35] However, recent theoretical work indicates that the actual Auger electron energies should be less than 52 eV, at 48.45 and 48.40 eV with a very small energy splitting.[36] Both the observed "Auger" peak energy of ~ 52 eV and the splitting (1.2 eV) are inconsistent with these calculated values. In addition, the intensity observed in the peaks near 52 eV is much too high to be consistent with the predicted 1% of dimer produced at this temperature.[44] The Auger inter-

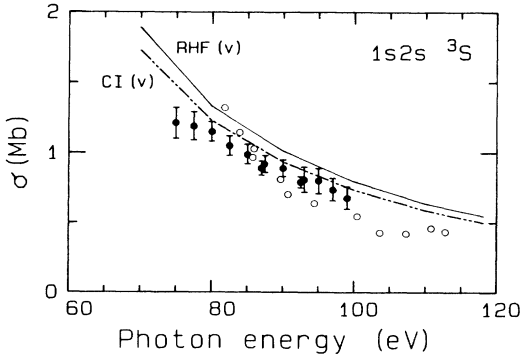

FIG. 7. Derived absolute cross section (Mb) for the $1s2s\ ^3S$ main line. Open circles are data from Gerard (no quoted error) (Ref. 35). Solid circles are "velocity" (V) theory by Larkins *et al.*, as labeled (Ref. 34).

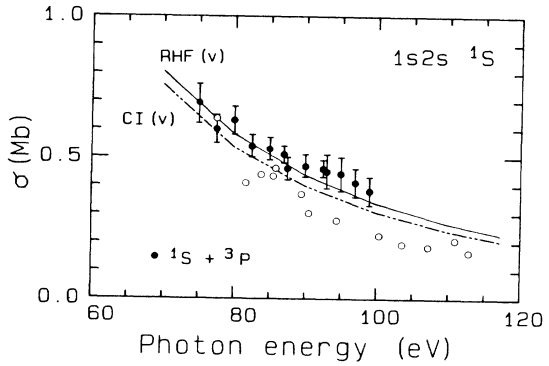

FIG. 8. Derived absolute cross section (Mb) for the sum of the $n=2\ ^1S$ and ^3P ionization are shown by dark circles for our results. Theory curves (Ref. 34) and Gerard's data (Ref. 35) are same as in Fig. 7, but represent only the main-line cross section (^1S).

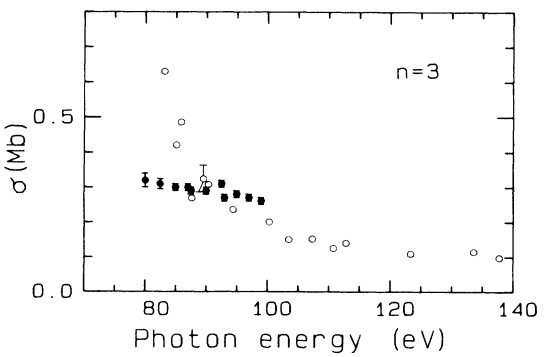

FIG. 9. Derived absolute cross section (Mb) for the $n=3$ satellites ($1s3l$). Gerard data are shown as open circles, with one representative error bar (Ref. 35).

pretation would thus require a postulation that the molecular ionization cross section is much larger than twice the atomic cross section, or that the amount of Li_2 significantly exceeds 1%. Several calculations on the Li_2 molecule indicate that the molecular cross section is indeed roughly twice the atomic value at these energies, as expected.[31,48]

In light of these facts, Larkins *et al.*[36] have proposed that atom- or ion-molecule collisions, followed by molecular autoionization, is responsible for the peaks near 52 eV kinetic energy in the Gerard spectra. The proposed three-step mechanism is as follows:

(1) Atomic excitation and ionization.

$$\mathrm{Li}(1s^2 2s)+h\nu \rightarrow \mathrm{Li}^*(1snln'l') , \tag{8}$$

$$\mathrm{Li}(1s^2 2s)+h\nu \rightarrow \mathrm{Li}^+(1snl)+e^- . \tag{9}$$

(2) Atom- or ion-molecule collisions.

$$\mathrm{Li}^*(1snln'l')+\mathrm{Li}_2(1\sigma^4 2\sigma_g^2) \rightarrow \mathrm{Li}(1s^2 2s) + \mathrm{Li}_2^*(1\sigma^3 2\sigma_g^2 n\phi^1) , \tag{10}$$

$$\mathrm{Li}^+(1snl)+\mathrm{Li}_2(1\sigma^4 2\sigma_g^2) \rightarrow \mathrm{Li}^+(1s^2) + \mathrm{Li}_2^*(1\sigma^3 2\sigma_g^2 n\phi^1) . \tag{11}$$

(3) Molecular autoionization.

$$\mathrm{Li}_2^*(1\sigma^3 2\sigma_g^2 n\phi^1) \rightarrow \mathrm{Li}_2^+(1\sigma^4 2\sigma_g)+e^- . \tag{12}$$

The autoionizing processes in Eq. (12) where $n\phi$ corresponds to $1\pi_u$, $2\sigma_u$, $2\sigma_g$, and $1\pi_g$ have been observed with electron kinetic energies of 51.5, 51.6, 52.8, and 53.9 eV,[49] in excellent agreement with the energies observed by Gerard (51.6 and 52.8 eV).[35]

We believe that the collisional model put forth by Larkin *et al.*[36] is very probably correct, requiring only that atom- or ion-molecule collision cross sections be 1 to 2 orders of magnitude higher than photoionization cross sections, which is quite possible.[50,51] This interpretation also suggests reanalysis of Gerard's data with little or no correction for dimer intensity, which should only contribute $\sim 2\%$ to the intensity of the atomic photoemission peaks.

IV. RESONANT RESULTS

In Sec. IV A we briefly review the Fano formalism for autoionizing total cross-section profiles and give a brief description of the Starace parameters, which apply to partial cross sections. In Sec. IV B we present the data analysis. A discussion of the results at the $[1s(3s3p)^3P]^2P$ resonance in Li follows in Sec. IV C.

A. Theoretical background

Fano first described the effect of an isolated discrete state ϕ on the total photoabsorption cross section.[52] A discrete state is embedded in one or more continua leading to oscillations in the total ionization cross section caused by interference between the two indistinguishable pathways: direct ionization and autoionization via the discrete level. For an isolated resonance, Fano expressed the total cross section (σ_t) in terms of a nonresonant "background" cross section (σ_0) as

$$\sigma_t = \sigma_0 \left[\rho^2 \frac{(q+\varepsilon)^2}{1+\varepsilon^2} + 1 - \rho^2 \right] , \tag{13}$$

with

$$\varepsilon = \frac{E - E_0}{\Gamma/2} . \tag{14}$$

Here ρ^2 and q are Fano parameters (assumed constant over the resonance) which describe the strength and shape of the resonant profile, E is the photon energy, E_0 is the resonant energy, Γ is the linewidth (FWHM), and ε is a reduced energy.

Furthermore, ρ^2, q, σ_0, and Γ can be expressed in terms of dipole and Coulomb matrix elements connecting the ground (g), discrete (ϕ), and continuum (μ) wave functions. The correlation coefficient ρ^2 is a measure of the strength of the resonance and corresponds to the relative decrease below the background cross section σ_0. In terms of matrix elements,

$$\rho^2 = \frac{\sum_\mu |\langle \phi | V | \mu \rangle \langle \mu | \mathbf{r} | g \rangle|^2}{\sum_\mu |\langle \phi | V | \mu \rangle|^2 \sum_\mu |\langle \mu | \mathbf{r} | g \rangle|^2} , \tag{15}$$

where V and $\mathbf{r}$ are the Coulomb and dipole operators. The q parameter describes the shape of the resonant profile which can be of a Lorentzian, asymmetric, or window type, and is expressed as

$$q = \frac{\langle \Phi | \mathbf{r} | g \rangle}{\pi \sum_\mu \langle \phi | V | \mu \rangle \langle \mu | \mathbf{r} | g \rangle} , \tag{16}$$

where Φ is now the discrete state modified by the continua. The maximum relative increase in the cross section in the vicinity of the resonance is equal to $\rho^2 q^2$. The matrix elements in Eqs. (15) and (16) vary slowly with energy; thus ρ^2 and q are relatively constant over the width of the resonance.

The nonresonant background cross section σ_0 is simply

$$\sigma_0 = \sum_\mu |\langle \mu | \mathbf{r} | g \rangle|^2 \tag{17}$$

and the linewidth Γ of the resonance is given by

$$\Gamma = 2\pi \sum_\mu |\langle \phi | V | \mu \rangle|^2 . \tag{18}$$

The above formalism, though appropriate for describing the total cross section, does not apply to individual partial cross sections. Several workers, including Davis and Feldkamp,[53] Combet Farnoux,[54] and Starace,[55] have derived equivalent expressions to describe decay into several continuum channels. Using the notation of Starace, an individual *observable* cross section $\sigma(\mu)$ can be written as

$$\sigma(\mu)=\frac{\sigma_0(\mu)}{1+\varepsilon^2}\{\varepsilon^2+2[q\ \mathrm{Re}(\alpha_\mu)-\mathrm{Im}(\alpha_\mu)]\varepsilon+1$$
$$-2q\ \mathrm{Im}(\alpha_\mu)-2\,\mathrm{Re}(\alpha_\mu)+(q^2+1)\,|\,\alpha_\mu\,|^2\}\ , \tag{19}$$

where $\sigma_0(\mu)$ is the nonresonant partial cross section for the μth observable final state, and ε and q are defined in Eqs. (14) and (16), respectively. The complex parameter α_μ is given by[56]

$$\alpha_\mu=\frac{\langle\phi\,|\,V\,|\,\mu\rangle}{\langle g\,|\,\mathbf{r}\,|\,\mu\rangle}\left[\frac{2\pi}{\Gamma}\sum_\mu\langle g\,|\,\mathbf{r}\,|\,\mu\rangle\langle\mu\,|\,V\,|\,\phi\rangle\right], \tag{20}$$

where Γ is given in Eq. (18). The term in parentheses is common to all channels μ. The Starace formalism retains the use of q to describe the total cross-section profile shape; the squares of the α_μ parameters for each channel are similar to the Fano ρ^2 parameter and an indication of the resonant strength per channel.

The Fano and Starace formalisms lead to the same mathematical form for the total cross section,

$$\sigma_t=\sigma_0\left[\frac{C_1+C_2\varepsilon+\varepsilon^2}{1+\varepsilon^2}\right], \tag{21}$$

where the Starace C_1 and C_2 parameters can be expressed in terms of q and ρ^2 as

$$C_1=\rho^2(q^2-1)+1\ , \tag{22}$$
$$C_2=2q\rho^2\ . \tag{23}$$

However, the ρ^2 matrix-element expression in Eq. (15) is not correct for partial cross-section profiles.

For the $1s(3s3p)$ resonance in atomic Li, we report both Fano (q and ρ^2) and Starace (C_1 and C_2) parameters for the total and partial cross sections. Because our resonant results are for the most part qualitative, we refer the reader to other sources for more details on the derivations for the Fano and Starace formalisms.[11,12,43,52,55]

B. Data analysis

A TOF spectrum taken at $\theta=54.7°$ and on the $1s(3s3p)\,^3P$ resonance at 71.2 eV is shown in Fig. 10. The spectrum is uncorrected for the analyzer transmission, which decreases at lower kinetic energy. The $1s2s\,^1S$ main line and $1s2p\,^3P$ satellite are unresolved; therefore, their summed intensity was used for the fitting procedures described below.

The total and partial cross-section profiles (with the exception of the $1s2p\,^1P$ state) in the vicinity of the $1s(3s3p)\,^3P$ resonance were fitted to the Fano functional form of Eq. (13) convoluted with a Gaussian of 0.20 eV FWHM for the monochromator bandpass. The Fano function was used for the partial cross sections for ease of fitting, though the inferred Starace parameters in Table V are more strictly correct. A resonant energy of 71.186 eV was used for the fitting compared with the energy in photoabsorption[37] of 71.14 eV, and the resonance linewidth Γ was taken as 0.10 eV from experiment[30] and theory.[57] The $1s2p\,^1P$ cross-section profile was fitted to a Lorentzian of 0.10 eV FWHM convoluted with a Gaussian of 0.20 eV FWHM. The resulting Fano q and ρ^2 values and the Starace C_1 and C_2 parameters are reported in Table V. The fits are plotted along with the data in Figs. 11 and 12.

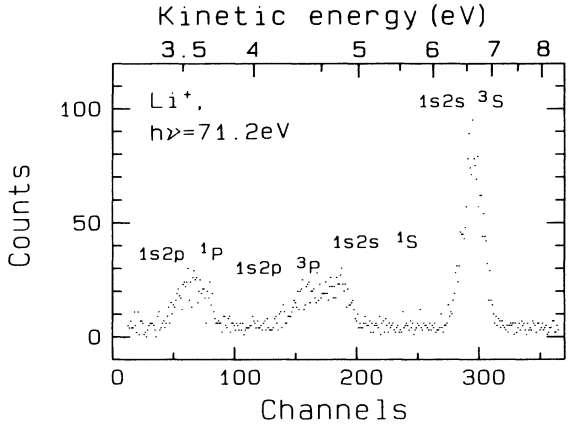

FIG. 10. TOF photoelectron spectrum taken at $h\nu=71.2$ eV and $\theta=54.7°$ on the $[1s(3s3p)^3P]^2P$ doubly excited resonance.

In all cases the nonresonant background cross section σ_0 was taken to be a linear function of energy. Since there are relatively few data points over the resonance, we emphasize that the fitting parameters contain appreciable error, as quoted in Table V. Errors in the Fano and Starace parameters include uncertainty in determining the best fit and in the selection of a background cross section σ_0.

One complication in the data analysis involves the presence of a small resonance at only ~ 0.3 eV higher energy, assigned as the ^1P component. Though this resonance appears to be quite small in the total photoabsorption cross section (see Fig. 11, solid curve),[30] its presence could perturb the partial cross sections to varying extents in the vicinity of the ^3P resonance. This second resonance at 71.47 eV (Ref. 37) has been ignored in our fits due to the scarcity of data in this region and the small effect on the cross sections. We note that one of our data points lies at 71.5 eV, which is about the center of this second resonance and high throughout Figs. 11 and 12.

C. Discussion of resonance results

Though we have thus far referred to the resonance at 71.14 eV as the doubly excited configuration $[1s(3s3p)\,^3P]^2P$, it is well known that the series of states leading to the Li $n=3$ satellite thresholds are not the expected simple Rydberg series, but rather configurationally mixed series.[30] The analogous doubly excited states in He have been studied extensively both experimentally[8,11] and theoretically.[21,22,57–62] In He the strongly interacting series of resonances have been

TABLE V. Fano and Starace parameters for the total and partial cross sections for the $1s(3s3p)^3P$ resonance.

Channel	Fano parameters q	Fano parameters ρ^2	Starace parameters C_1	Starace parameters C_2
Total	−3.2(7)	0.20(8)		
	−2.60[a]	0.144[a]		
$1s2s\ ^3S$	−1.6(3)	0.60(15)	1.9(6)	−1.9(6)
$1s2s\ ^1S + 1s2p\ ^3P$	−2.5(10)	0.25(15)	2.3(15)	−1.3(9)
$1s2p\ ^1P$	Lorentzian			

[a]Values from Ref. 30.

classified with several schemes.[57,60,62,63] More recently, the resonances below the $n=3$ satellite thresholds in Li have been classified in parallel to He, with reasonable success.[30] We shall use here the notation of Lipsky *et al.*,[58] consistent with the first analysis of the $n=3$ resonances in Li.

The Lipsky notation $(N,n\alpha)^{1,3}P$ identifies resonances by principal quantum number (N), outer quantum number (n), and series label (α).[58] The label α (where the lowest series is termed a) was obtained from approximately constant quantum defects or from configurations of the wave functions. The 71.14-eV resonance is labeled $[(3,3a)^3P]^2P$, and is the first member of the ^3P a series. We note that in the doubly excited symmetry basis (DESB) of Herrick and Sinanoğlu,[57] this resonance is labeled as K_n, or 2_3 for helium.

Our resonant profile parameters for the total cross section agree within error limits with a previous photoabsorption measurement, showing some asymmetry in shape indicated by a small negative q parameter.[30] Figure 11 includes the convoluted and deconvoluted fits to our data, and a photoabsorption curve (0.027-eV bandpass).[30] Though our ρ^2 and q agree within errors with the values reported for the photoabsorption data (see Table V),[30] the plotted curves in Fig. 11 appear to be significantly different in magnitude. The relative increase at the resonance is equal to $\rho^2 q^2$, which is twice as large as for our plotted fit (deconvoluted) compared to the absorption curve.[30] We note that an earlier photoabsorption measurement[26] disagrees with both our data and the more recent photoabsorption curve,[30] showing an even larger positive effect at the resonance (a more negative q parameter). We offer no explanation for these discrepancies.

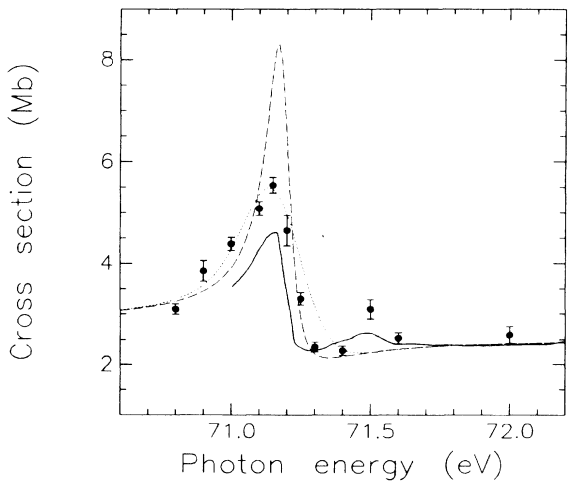

FIG. 11. Total photoabsorption cross section over the $1s(3s3p)$ resonance. The dashed curves are convoluted (small dashed) and deconvoluted (large dashed) fits to our data (dark circles) using a Fano profile where $\rho^2=0.20$ and $q=-3.24$. The fitted curves have been scaled to the photoabsorption curve (Ref. 30) (solid) at 72 eV. A Gaussian of width 0.20 eV (FWHM) was used for monochromator bandpass in the deconvoluted fit. The natural linewidth of the resonance was taken from photoabsorption data (Ref. 30) which is confirmed by theory (Ref. 57) as being equal to 0.10 eV.

For the individual profiles (Fig. 12), we can make the following generalizations. The main-line profiles ($^{1,3}S$) appear to be asymmetric, while the $n=2$ satellite profiles ($^{1,3}P$) are probably nearly Lorentzian. The $1s2s\ ^3S$ and $1s2p\ ^1P$ profiles shapes support this statement unambiguously. For the summed ^1S and ^3P profile, careful examination of the spectra reveals that the ^1S intensity maximum is at 71.15 eV in our data, whereas the ^3P maximum is at 71.20 eV. Furthermore, the ^1S intensity is at a maximum and below the nonresonant intensity level at 71.3 eV. Qualitatively, this indicates some asymmetry in the ^1S main-line profile and very little if any asymmetry in the ^3P profile. Although this behavior was obvious to visual inspection, we did not proceed with further deconvolution because of the limited accuracy of this data set. Higher resolution and higher count rates are needed to confirm these ^1S and ^3P profiles quantitatively.

Asymmetry in a line profile indicates the degree of interference and coupling between the discrete and continuum states. Examining the expression for the Fano q parameter in Eq. (16), we see that a small value of q (corresponding to an asymmetric profile) can be caused in part by a large amount of coupling between the discrete and continuum states, through the matrix element $\langle\phi \mid V \mid \mu\rangle$. This Fano q parameter applies only to the total cross section; thus it is more difficult to make simple generalizations about the individual profiles. An asymmetric shape generally indicates strong coupling, but it is also influenced by the background cross section. For the $1s2p$ satellites in Li the nonresonant intensity is so small that if the resonance is to have an appreciable

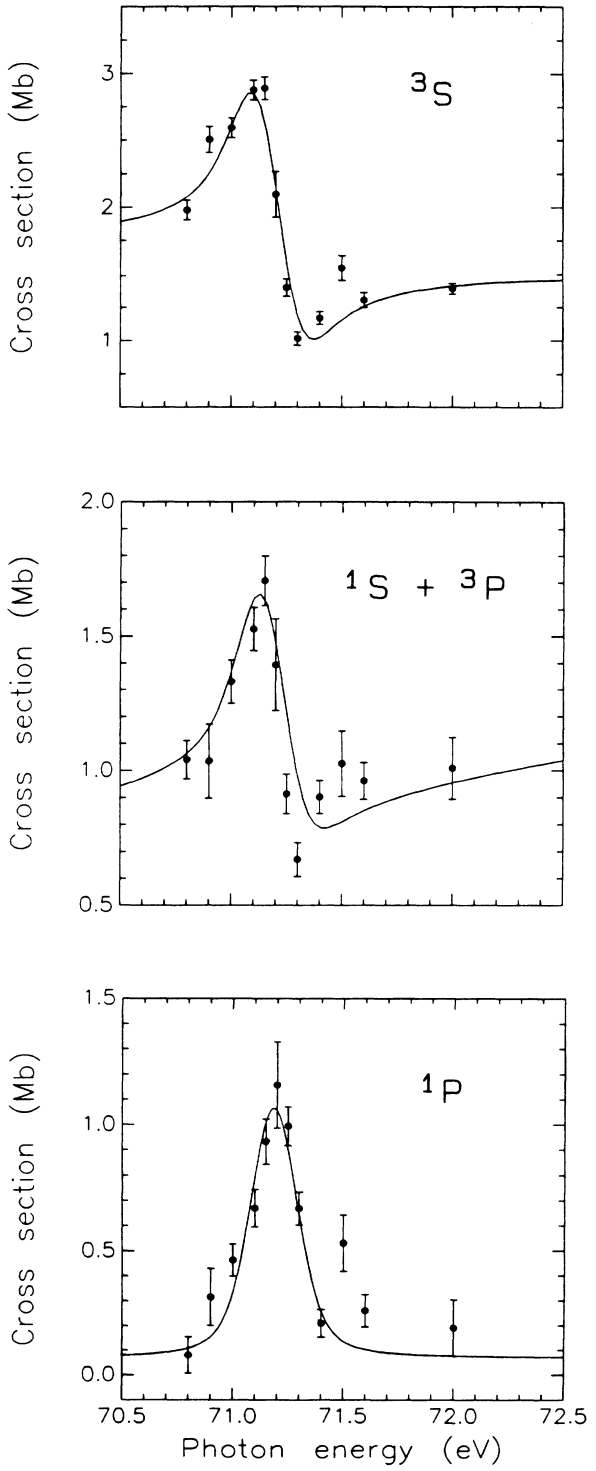

FIG. 12. Individual relative cross sections for resonant decay to the $n=2$ states ^3S (top), $^1S+{}^3P$ (middle), and ^1P (bottom). The solid circles in the top and middle panels are fits to the data using the Fano formula with a width of 0.10 eV convoluted with a Gaussian of 0.20 eV FWHM (monochromator bandpass). The resulting Fano parameters are shown in Table V. For the ^1P profile (bottom), the data were fit to a Lorentzian (0.10 eV FWHM) convoluted with a Gaussian (0.20 eV FWHM).

effect, only a symmetric Lorentzian profile is possible, as observed. For the $1s2s$ main lines, there is enough nonresonant cross section to interfere strongly with the autoionization pathway via the discrete state. Calculations are needed, similar to those on He,[21,22] to describe in detail the degree of coupling between the ground, discrete, and continuum states at this resonance.

We now comment briefly on the cross-section results of Gerard[35] at this resonance. Their photon resolution was 0.30 eV compared with our bandpass of 0.20 eV. The larger bandpass affects their spectrum at $h\nu=71.28$ eV, in which each peak appears as a doublet; some of the cross-section structure is starting to appear in the peaks. Thus, aside from any possible complications from molecular Li_2, the large bandpass prohibits a detailed quantitative study of the resonance profiles. This is emphasized by the lack of agreement with our results. For example, the Gerard data[35] for the $1s2s$ ^3S profile show very little if any asymmetry.

Because the doubly excited state $3s3p$ in He has been studied extensively,[8,11,21,22,57–63] we compare it with the $[1s(3s3p)^3P]^2P$ resonance in Li. For the total cross sections, the "phase" of the resonance (determined by the sign of the Fano q parameter) is opposite for He (Refs. 8 and 11) and Li. Fano and Cooper presented arguments to explain the sign of q for the $2s2p$ and $3s3p$ resonances in He.[47] The Fano q parameter is related to the dipole and Coulomb matrix elements between the ground, discrete, and continuum states, as in Eq. (16). The sign of q then is determined by the signs of these matrix elements. For example, the predicted negative q for the He $2s2p$ resonance was found to depend on a single negative matrix element $\langle 2s2p \mid \mathbf{r} \mid 1s^2 \rangle$. When this element is approximated with one-electron integrals as

$$\langle 2s2p \mid \mathbf{r} \mid 1s^2 \rangle \sim (2)^{1/2} \langle 2s \mid 1s \rangle \langle 2p \mid \mathbf{r} \mid 1s \rangle , \quad (24)$$

Fano and Cooper concluded that it was the negative sign of $\langle 2s \mid 1s \rangle$ which ultimately produced a negative q parameter, with all other matrix elements in Eq. (16) positive. The negative sign of the overlap integral $\langle 2s \mid 1s \rangle$ was explained by less screening of the $2s$ electron in the $2s2p$ state relative to the $1s$ electron in $1s^2$. We use this reasoning below to rationalize that the double-excitation dipole integrals are negative. Similar arguments were made to predict the positive q for the He $3s3p$ resonance.[47]

If we proceed to make parallel arguments for the $1s(3s3p)$ resonance in Li, we first need to estimate the inverse of the q parameter as sums over the different continuum channels:

$$q^{-1}_{(1s3s3p)} = \frac{\pi \langle 1s3s3p \mid V \mid 1s^2\varepsilon p \rangle \langle 1s^2\varepsilon p \mid \mathbf{r} \mid 1s^2 2s \rangle}{\langle 1s3s3p \mid \mathbf{r} \mid 1s^2 2s \rangle} + \frac{\pi \langle 1s3s3p \mid V \mid 1s2s\varepsilon p \rangle \langle 1s2s\varepsilon p \mid \mathbf{r} \mid 1s^2 2s \rangle}{\langle 1s3s3p \mid \mathbf{r} \mid 1s^2 2s \rangle} + \frac{\pi \langle 1s3s3p \mid V \mid 1s2p\varepsilon s \rangle \langle 1s2p\varepsilon s \mid \mathbf{r} \mid 1s^2 2s \rangle}{\langle 1s3s3p \mid \mathbf{r} \mid 1s^2 2s \rangle} , \quad (25)$$

where we have ignored the $^{1,3}S$ and $^{1,3}P$ splittings for the

$1s2s$ and $1s2p$ states and have assumed that the modified discrete state Φ is approximately equal to the unperturbed state ϕ. If we further use the fact that the $1s^2$ cross section is very small at the resonance,[34,35] and thus contributes little to the shape of the total cross section, we can neglect the first term in Eq. (25) above.

We are now left with estimating the signs of the following matrix elements:

$$\langle 1s3s3p \mid V \mid 1s2s\varepsilon p \rangle \quad \langle 1s2s\varepsilon p \mid \mathbf{r} \mid 1s^2 2s \rangle$$

$$\langle 1s3s3p \mid V \mid 1s2p\varepsilon s \rangle \quad \langle 1s2p\varepsilon s \mid \mathbf{r} \mid 1s^2 2s \rangle$$

$$\langle 1s3s3p \mid \mathbf{r} \mid 1s^2 2s \rangle .$$

The first two Coulomb matrix elements above (left column) are assumed positive based on the convention that radial wave functions are positive when the electrons are near the nucleus. The next two dipole matrix elements (right column) between the ground and continuum states are, respectively, positive for the $1s2s\varepsilon p$ continuum (a single-excitation dipole) and possibly negative for the $1s2p\varepsilon s$ continuum (a double-excitation dipole). The last remaining integral involves a double excitation and is thus negative. Combining all these signs, we predict that the q parameter is probably negative, as observed, for the $1s3s3p$ resonance.

V. CONCLUSIONS

We have presented the first experimental results on the core ionization of atomic Li which are uncomplicated by the presence of Li_2 or collisional processes. The nonresonant results indicate that theory at the relaxed Hartree-Fock level is probably adequate to model the $1s2s$ main-line cross section for atomic Li. The Gerard experimental cross sections[35] for the main lines have a somewhat different slope for the decrease of the curves with energy. Our low-resolution results prohibit a detailed study of the $1s2p$ conjugate shakeup satellites, though relative intensities were obtained at a few energies for the ^1P satellite. The summed $n=3$ satellites were monitored from 5 to 25 eV above threshold, and cross-section results disagree with those of Gerard.[35] A reanalysis of those data[35] for all peaks assuming a collisional interpretation[36] for the origin of the 52-eV "Auger" peaks is warranted. Theory which reliably predicts the $n=2$ and $n=3$ satellite intensities as a function of energy should provide a basis for understanding electron correlation in atomic Li.

Our results at the $[(3,3a)^3P]^2P$ doubly excited resonance are in good agreement with previous photoabsorption measurements,[30] confirming an asymmetric profile in the total cross section. We have also measured partial cross sections over this resonance, with the qualitative result that the $1s2s\ ^{1,3}S$ main lines show asymmetric shapes while the $1s2p\ ^{1,3}P$ satellites have nearly Lorentzian profiles. At present there are no calculations on the $[(3,3a)^3P]^3P$ resonance in Li. Just recently, theoretical results on the analogous $3s3p$ state in He were reported,[21,22] in excellent agreement with experiment.[11,12] It is hoped that the experimental results presented here for Li will stimulate calculations on the individual cross-section profiles at resonances below the $n=3$ and higher satellite thresholds in this open-shell system.

ACKNOWLEDGMENTS

We are gratefully acknowledge very helpful discussions with F. P. Larkin and J. Cooper. This work was supported by the Director, Office of Energy Research, Office of Basic Energy Sciences, Chemical Sciences Division, of the U.S. Department of Energy under Contract No. DE-AC03-76SF00098. It was performed at the Stanford Synchrotron Radiation Laboratory, which is supported by the Department of Energy's Office of Basic Energy Sciences.

*Present address: National Bureau of Standards, Gaithersburg, MD 20899.

†Present address: Technische Universität München, D-8046 Garching b., München, Federal Republic of Germany.

‡Permanent address: Institut für Atom- und Festkörperphysik, Freie Universität Berlin, Arnimallee 14, D-1000 Berlin 33, West Germany.

§Permanent address: Technische Universität Berlin, Institut für Strahlungs- und Kernphysik, Sekr. PN 3-2, Hardensbergstrasse 36, D-1000 Berlin 12, West Germany.

[1]T. A. Carlson, Phys. Rev. **156**, 142 (1967).

[2]J. A. R. Samson, Phys. Rev. Lett. **22**, 693 (1969).

[3]T. A. Carlson, M. O. Krause, and W. E. Moddeman, J. Phys. (Paris) Colloq. **32**, C4-76 (1971).

[4]M. O. Krause and F. Wuilleumier, J. Phys. B **5**, L143 (1972).

[5]P. R. Woodruff and J. A. R. Samson, Phys. Rev. Lett. **45**, 110 (1980).

[6]F. Wuilleumier, M. Y. Adam, N. Sandner, and V. Schmidt, J. Phys. (Paris) Lett. **41**, L373 (1980).

[7]J. M. Bizau, F. Wuilleumier, P. Dhez, D. L. Ederer, T. N. Chang, S. Krummacher, and V. Schmidt, Phys. Rev. Lett. **48**, 588 (1982).

[8]P. R. Woodruff and J. A. R. Samson, Phys. Rev. A **25**, 848 (1982).

[9]V. Schmidt, H. Derenbach, and R. Malutzki, J. Phys. B **15**, L523 (1982).

[10]P. Morin, M. Y. Adam, I. Nenner, J. Delwiche, M. J. Hubin-Franskin, and P. Lablanquie, Nucl. Instrum. Methods **208**, 761 (1983).

[11]D. W. Lindle, T. A. Ferrett, U. Becker, P. H. Kobrin, C. M. Truesdale, H. G. Kerkhoff, and D. A. Shirley, Phys. Rev. A **31**, 714 (1985).

[12]D. W. Lindle, T. A. Ferrett, P. A. Heimann, and D. A. Shirley, Phys. Rev. A **36**, 2112 (1987); D. W. Lindle, P. A. Heimann, T. A. Ferrett, and D. A. Shirley, *ibid.* **35**, 1128 (1987).

[13]E. E. Salpeter and M. H. Zaidi, Phys. Rev. **125**, 248 (1962).

[14]R. L. Brown, Phys. Rev. A **1**, 341 (1970).

[15]V. Jacobs, Phys. Rev. A **3**, 289 (1971).
[16]V. L. Jacobs and P. G. Burke, J. Phys. B **5**, L67 (1972).
[17]T. N. Chang, J. Phys. B **13**, L551 (1980).
[18]J. A. Richards, B.S. honours thesis, Monash University, Australia, 1981.
[19]K. A. Berrington, P. G. Burke, W. C. Fon, and K. T. Taylor, J. Phys. B **15**, L603 (1982); see P. C. Ojha, *ibid.* **17**, 1807 (1984) for additional discussion.
[20]J. A. Richards and F. P. Larkins, J. Electron Spectrosc. **32**, 193 (1983).
[21]S. Salomonson, S. L. Carter, and H. P. Kelly, J. Phys. B **18**, L149 (1985).
[22]H. P. Kelly, Phys. Scr. (to be published).
[23]G. V. Marr, Proc. Phys. Soc. London **81**, 9 (1963).
[24]R. D. Hudson and V. L. Carter, Phys. Rev. **137**, A1648 (1965); J. Opt. Soc. Am. **57**, 651 (1967).
[25]M. Ya. Amusia, N. A. Cheropkov, Dj. Živanović, and V. Radojević, Phys. Rev. A **13**, 1466 (1976).
[26]G. Mehlman, D. L. Ederer, E. B. Saloman, and J. W. Cooper, J. Phys. B **11**, L689 (1978).
[27]J. W. Cooper, M. J. Conneely, K. Smith, and S. Ormonde, Phys. Rev. Lett. **22**, 1540 (1970).
[28]D. L. Ederer, T. Lucatorto, and R. P. Madden, Phys. Rev. Lett. **25**, 1537 (1970).
[29]D. L. Ederer, T. Lucatorto, and R. P. Madden, J. Phys. (Paris) Colloq. **32**, C4-85 (1971).
[30]G. Mehlman, J. W. Cooper, and E. B. Saloman, Phys. Rev. A **25**, 2113 (1982).
[31]S. Krummacher, V. Schmidt, J. M. Bizau, D. L. Ederer, P. Dhez, and F. Wuilleumier, J. Phys. B **15**, 4264 (1982).
[32]F. P. Larkins, P. D. Adeney, and K. G. Dyall, J. Electron Spectrosc. **22**, 141 (1981).
[33]G. De Alti, P. Decleava, and A. Lisini, Chem. Phys. **80**, 229 (1983).
[34]F. P. Larkins, B. I. Craig, and J. A. Richards (unpublished).
[35]P. Gerard, Ph.D. thesis, Université de Paris-Sud, 1984.
[36]F. P. Larkins and J. A. Richards, Aust. J. Phys. **39**, 1 (1986).
[37]A. M. Cantú, W. H. Parkinson, G. Tondello, and G. Tozzi, J. Opt. Soc. Am. **67**, 1030 (1977).
[38]M. G. White, R. A. Rosenberg, G. Gabor, E. D. Poliakoff, G. Thornton, S. Southworth, and D. A. Shirley, Rev. Sci. Instrum. **50**, 1288 (1979).
[39]S. Southworth, C. M. Truesdale, P. H. Kobrin, D. W. Lindle, W. D. Brewer, and D. A. Shirley, J. Chem. Phys. **76**, 143 (1982).
[40]S. Southworth, U. Becker, C. M. Truesdale, P. H. Kobrin, D. W. Lindle, S. Owaki, and D. A. Shirley, Phys. Rev. A **28**, 261 (1983).
[41]F. Wuilleumier, and M. O. Krause, J. Electron Spectrosc. **15**, 15 (1979).
[42]P. H. Kobrin, Ph.D. thesis, University of California, Berkeley, 1983.
[43]P. H. Kobrin, U. Becker, S. Southworth, C. M. Truesdale, D. W. Lindle, and D. A. Shirley, Phys. Rev. A **26**, 842 (1982).
[44]A. N. Nesmeyanov, *Vapor Pressure of the Chemical Elements* (Elsevier, Amsterdam, 1963); T. B. Douglas, L. F. Epstein, J. L. Dever, and W. H. Howland, J. Am. Chem. Soc. **77**, 2144 (1955).
[45]K. Codling and R. P. Madden, Phys. Rev. Lett. **12**, 106 (1964).
[46]P. A. Heimann, U. Becker, H. G. Kerkhoff, B. Langer, D. Szostak, R. Wehlitz, D. W. Lindle, T. A. Ferrett, and D. A. Shirley, Phys. Rev. A **34**, 3782 (1986).
[47]U. Fano and J. W. Cooper, Phys. Rev. **137**, 1364 (1965).
[48]J. W. Davenport, G. J. Cosgrove, and A. Zangwill, J. Chem. Phys. **78**, 1095 (1983).
[49]W. H. E. Schwarz, W. Butscher, D. L. Ederer, T. B. Lucatorto, B. Ziegenbein, W. Mehlhorn, and H. Prompeler, J. Phys. B **11**, 591 (1978).
[50]U. Fano and W. Lichten, Phys. Rev. Lett. **14**, 627 (1965).
[51]F. P. Larkins, J. Phys. B **5**, 571 (1972).
[52]U. Fano, Phys. Rev. **124**, 1866 (1961).
[53]L. C. Davis and L. A. Feldkamp, Phys. Rev. B **15**, 2961 (1977); **23**, 6239 (1981).
[54]F. Combet Farnoux, Phys. Rev. A **25**, 287 (1982).
[55]A. F. Starace, Phys. Rev. A **16**, 231 (1977).
[56]P. C. Kemeny, J. A. R. Samson, and A. F. Starace, J. Phys. B **10**, L201 (1977).
[57]D. R. Herrick and O. Sinanoğlu, Phys. Rev. A **11**, 97 (1975).
[58]L. Lipsky, R. Anania, and M. J. Conneely, At. Data Nucl. Data Tables **20**, 127 (1977).
[59]R. S. Oberoi, J. Phys. B **5**, 1120 (1972).
[60]K. T. Chung, Phys. Rev. A **6**, 1809 (1972).
[61]W. C. Martin, J. Phys. Chem. Ref. Data **2**, 257 (1973).
[62]J. W. Cooper, U. Fano, and F. Prats, Phys. Rev. Lett. **10**, 518 (1963).
[63]J. Macek, J. Phys. B **1**, 831 (1968).
[64]C. Moore, *Atomic Energy Levels*, Natl. Bur. Stand. Ref. Data Ser., Natl. Bur. Stand. (U.S.) Circ. No. 35 (U.S. GPO, Washington, D.C., 1971), Vol. 1.